PN-type carrier-induced filter with modulatable extinction ratio

Qing Fang,[1,2,*] Xiaoguang Tu,[1] Junfeng Song,[1] Lianxi Jia,[1] Xianshu Luo,[1] Yan Yang,[1,3] Mingbin Yu,[1] and Guoqiang Lo[1]

[1]*Institute of Microelectronics, A*STAR (Agency of Science and Technology Research), 117685, Singapore*
[2]*Optoelectronic System Laboratory, Institute of Semiconductors, CAS, Beijing, 100083, China*
[3]*Novitas, Nanoelectronics Centre of Excellence, School of Electrical and Electronic Engineering, Nanyang Technological University, 639798, Singapore*
** fangq@ime.a-star.edu.sg*

Abstract: We demonstrate the first PN-type carrier-induced silicon waveguide Bragg grating filter on a SOI wafer. The optical extinction ratio of this kind of filter can be efficiently modulated under both reverse and forward biases. The carrier-induced Bragg grating based on a PN junction is fabricated on the silicon waveguide using litho compensation technology. The measured optical bandwidth and the extinction ratio of the filter are 0.45 nm and 19 dB, respectively. The optical extinction ratio modulation under the reverse bias is more than 11.5 dB and it is more than 10 dB under the forward bias. Only 1-dB optical transmission loss is realized in this Bragg grating under a reverse bias. The shifting rates of the central wavelength under forward and reverse biases are ~-1.25 nm/V and 0.01 nm/V, respectively. The 3-dB modulation bandwidth of this filter is 5.1 GHz at a bias of −10 V.

OCIS codes: (130.0250) Optoelectronics; (050.2770) Gratings; (130.3120) Integrated optics devices.

References and links

1. K. O. Hill and G. Meltz, "Fiber Bragg grating technology fundamentals and overview," J. Lightwave Technol. **15**(8), 1263–1276 (1997).
2. A. D. Kersey, T. A. Berkoff, and W. W. Morey, "Multiplexed fiber Bragg grating strain-sensor system with a fiber Fabry - Perot wavelength filter," Opt. Lett. **18**(16), 1370–1372 (1993).
3. C. Y. Lin and L. A. Wang, "A wavelength- and loss- tunable band-rejection filter based on corrugated long-period fiber grating," IEEE Photon. Technol. Lett. **13**(4), 332–334 (2001).
4. W. Liang, Y. Huang, Y. Xu, R. K. Lee, and A. Yariv, "Highly sensitive fiber Bragg grating refractive index sensors," Appl. Phys. Lett. **86**(15), 151122 (2005).
5. H. Tsuda, "Fiber Bragg grating vibration-sensing system, insensitive to Bragg wavelength and employing fiber ring laser," Opt. Lett. **35**(14), 2349–2351 (2010).
6. Y. G. Han and S. B. Lee, "Tunable dispersion compensator based on uniform fiber Bragg grating and its application to tunable pulse repetition-rate multiplication," Opt. Express **13**(23), 9224–9229 (2005).
7. I. Giuntoni, A. Gajda, M. Krause, R. Steingrüber, J. Bruns, and K. Petermann, "Tunable Bragg reflectors on silicon-on-insulator rib waveguides," Opt. Express **17**(21), 18518–18524 (2009).
8. J. Brouckaert, W. Bogaerts, S. Selvaraja, P. Dumon, R. Baets, and D. V. Thourhout, "Planar concave grating demultiplexer with high reflective Bragg reflector facets," IEEE Photon. Technol. Lett. **20**(4), 309–311 (2008).
9. R. M. Parker, J. C. Gates, M. C. Grossel, and P. G. R. Smith, "In vacuo measurement of the sensitivity limit of planar Bragg grating sensors for monolayer detection," Appl. Phys. Lett. **95**(17), 173306 (2009).
10. G. Jiang, R. Chen, Q. Zhou, J. Yang, M. Wang, and X. Jiang, "Slab-modulated sidewall Bragg grating in silicon-on-insulator ridge waveguides," IEEE Photon. Technol. Lett. **23**(1), 6–8 (2011).
11. J. M. Castro, D. F. Geraghty, S. Honkanen, C. M. Greiner, D. Iazikov, and T. W. Mossberg, "Optical add-drop multiplexers based on the antisymmetric waveguide Bragg grating," Appl. Opt. **45**(6), 1236–1243 (2006).
12. D. T. H. Tan, K. Ikeda, and Y. Fainman, "Cladding-modulated Bragg gratings in silicon waveguides," Opt. Lett. **34**(9), 1357–1359 (2009).
13. S. Honda, Z. Wu, J. Matsui, K. Utaka, T. Edura, M. Tokuda, K. Tsutsui, and Y. Wada, "Largely-tunable wideband Bragg gratings fabricated on SOI ridge waveguides employed by deep-RIE," Electron. Lett. **43**(11), 630–631 (2007).

14. Q. Fang, J. F. Song, X. G. Tu, L. X. Jia, X. S. Luo, M. B. Yu, and G. Q. Lo, "Carrer-induced silicon Bragg grating filters with a p-i-n junction," IEEE Photon. Technol. Lett. **25**(9), 810–812 (2013).
15. Q. Fang, J. F. Song, X. S. Luo, L. X. Jia, M. B. Yu. G. Q. Lo, and Y. L. Liu, "High efficiency ring-resonator filter with NiSi heater," IEEE Photon. Technol. Lett. **24**(5), 350–352 (2012).

1. Introduction

Bragg grating is a grating with a periodic perturbation of the refractive index along the transmission direction of guide wave. Fiber Bragg grating filter has been applied widely in optical communications systems, which is specially used as filters, sensors and dispersion compensators [1–6]. Due to the monolithic integration and low cost of silicon-based devices, silicon photonics has become a promising prospect of research. Silicon-based Bragg grating had also been reported in the last decade [7–13]. Moreover, it is easy to realize the high speed modulation on the silicon-based Bragg grating devices by using a PN-type or PIN-type junction structure. However, these silicon-based Bragg gratings are formed by an etching technology. This kind of Bragg grating structure is permanent. The extinction ratio (ER) of the reflection wavelength of the above Bragg gratings is hard to obviously be changed and the reflection wavelength can only shift by the thermo-optic or electro-optic modulation. In the last year, we presented a PIN-type carrier-induced Bragg grating filter by using an implantation technology and it is realized to effectively modulate the extinction ratio under the forward bias [14]. However, it is hard to modulate the extinction ratio under the reverse bias because of the p-i-n junction structure.

In this letter, we present the first demonstration of a carrier-induced Bragg grating based on a PN-type junction on the ridge silicon waveguide by ion implantation technology. The optical bandwidth and the ER of the grating filter are 0.45 nm and 19 dB, respectively. With the carrier injection, the ER modulation is more than 10 dB. With the carrier depletion, the ER modulation is more than 11.5 dB. The average central wavelength shifting rates under forward and reverse biases are ~-1.25 nm/V and 0.01 nm/V, respectively. The optical loss is low with an operation of reverse bias. Only 1dB optical transmission loss of this Bragg grating is realized under a reverse bias. This kind of carrier-induced Bragg grating shifts the reflected wavelength under the bias and reduces the extinction ratio as well. It can be used as a special tunable filter or switch in wavelength-division multiplexed (WDM) systems. In principle, it can guide all waves as a normal waveguide with a reverse bias and filter a special wave without any bias.

2. Device's design and fabrication

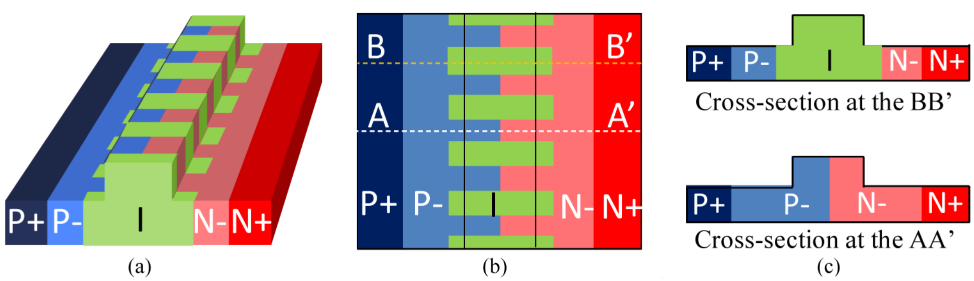

Fig. 1. Three-dimensional (3D) structure for the Bragg grating. (a) Three-dimensional (3D) structure of Bragg grating with a PN junction. (b) Top view of the Bragg grating. (c) Cross-sections of the Bragg grating at the AA' line and BB' line in (b).

The schematic structure of the carrier-induced Bragg grating filter is shown in Fig. 1. Figure 1(a) is the 3D structure of the PN-type carrier-induced Bragg grating filter. The fingers of P and N implantations form the PN junction, shown in Fig. 1(b) and the bottom of Fig. 1(c). And, each PN junction finger is separated by the intrinsic area, shown in Fig. 1(b) and the top of Fig. 1(c). The ridge width of silicon waveguide is 400 nm and the height of the ridge

#224043 - $15.00 USD Received 29 Sep 2014; revised 24 Oct 2014; accepted 31 Oct 2014; published 21 Nov 2014

waveguide is 220 nm. The slab height is 130 nm. According to the Bragg equation of $\lambda_0 = 2N_{eff}\Lambda$, the grating period Λ of 310 nm is designed for the operation in optical communications wavelength range, where λ_0 is the reflected wavelength of Bragg grating and N_{eff} is the effective refractive index of Bragg grating. The grating length is 2 mm. In order to simplify the process and reduce the lithography requirement, the duty cycle is 50:50. So, the length of the intrinsic pattern along the waveguide is 155nm. The length of each finger is designed based on the lithography precision. Figure 2(a) shows the actual length of the finger on the wafer after screen SiO2 etching process and its design length (red color) on the layout. The design length of a finger is 0.5um and the actual length on the wafer is 0.32um. It is a challenge for 248 nm lithography system to fully expose the grating pitch of 310 nm. Although the actual length of finger is shortened, the change of the finger centre position on the direction of light transmission is negligible. So, in order to get the intrinsic pattern width of 0.64um on the wafer and design the P/N interface of finger at the center of waveguide, the design compensation is needed, shown in Fig. 2(b). Both lengths of P/N fingers are the same, 0.5um. The overlapped width of P/N fingers is 180 nm in the design. The dark-yellow color represents the ridge of the waveguide. Based on the carrier plasma dispersion effect in silicon, the carrier concentration can effectively change the effective refractive index of silicon waveguide in the implantation area. We use ion implantation to form the Bragg grating pattern instead of silicon etching process usually used. This kind of Bragg grating filter is based on carrier concentration.

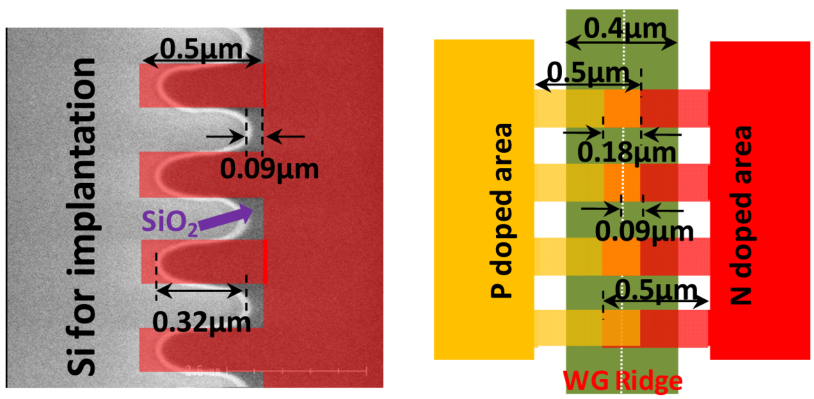

(a) (b)

Fig. 2. Compensation design for PN-type grating formation. (a) Designed/actual patterns of the finger (red color is the design pattern); (b) Compensation design on the layout, including 180 nm overlapped area.

The extinction ratio modulation is dominated by depletion width. For an PN-type junction, the depletion width (W) is given by

$$W = \left[\frac{2\varepsilon(V_{bi} - V)}{e}\left(\frac{N_a + N_d}{N_a N_d}\right)\right]^{1/2} \tag{1}$$

where V_{bi} is the built-in voltage of the junction, V is the external voltage, N_a is the carrier concentration of P-type, N_d is the carrier concentration of N-type. According to the above equation, the depletion width increases with the increase of the reverse bias and the depletion width decreases with the increase of the forward bias. So, when the Bragg grating is operated with the reverse bias, the grating finger will become shorter and the extinction ratio of the grating will become small. When the Bragg grating is operated with a high forward bias, the

#224043 - $15.00 USD Received 29 Sep 2014; revised 24 Oct 2014; accepted 31 Oct 2014; published 21 Nov 2014

current is so high that the profile of the grating becomes weaker, which also reduces the extinction ratio of the grating. The simulated depletion width at a PN-type junction using the above Eq. (1) is shown in Fig. 3, assuming that the implantation is uniform in the silicon waveguide. With the increase of reverse bias, the depletion width obviously increases, especially in the low implantation range. The simulated results show that the carrier can be swept out from the finger of the implantation area. Once the carriers are swept out under a reverse bias, this device has not the filter function anymore and it is changed to become a normal waveguide to guide all waves.

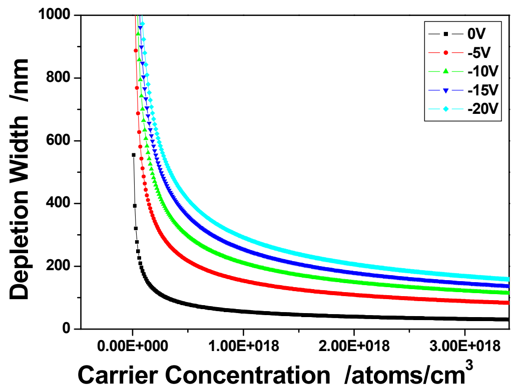

Fig. 3. Simulated depletion width of a PN junction under the reverse bias.

The carrier-induced Bragg grating was fabricated on eight inch SOI wafers with a 220nm-thick silicon epitaxial layer and a 2um-thick buried oxide layer. A 1500Å-thick SiO_2 layer was deposited as a screen layer for the P-type implantation. After the lithographic process of P-type implantation pattern for the left grating fingers shown in Fig. 1(b), the 1500Å-thick screen SiO_2 was partially etch by a dry etching technology and a 100Å-thick SiO_2 was remained. The scanning electron microscope (SEM) image of the formed screen SiO_2 finger is shown in Fig. 2(a). This 100Å-thick remained SiO_2 layer was designed to avoid silicon surface damage. It is critical to form the carrier-induced Bragg grating. In order to get a uniform implantation in the 220nm-thick silicon waveguide, two kinds of boron ion conditions were processed. The doses of 0.5×10^{13} ions/cm^2 and 1.5×10^{13} ions/cm^2 were designed, according to the simulated results using the software of SILVACO TCAD. The corresponding energies are 15 KeV and 35 KeV, respectively. The carrier concentration near the junction is around 7×10^{17} atoms/cm^3. There is a trade-off to design the implantation condition for both the extinction ratio of the grating and the depletion width of the P/N junction. Later, the photoresist and SiO_2 screen layer for P implantation were stripped. Another SiO_2 layer of 1500 Å was deposited and etched for the N-type implantation. Based on the similar processes, the phosphorus ion with the similar doses was implanted under the energies of 30 KeV and 90 KeV, respectively. Based on the compensation design for the implantation pattern in Fig. 2(b), a PN-type carrier-induced grating was formed. After the screen SiO_2 was stripped, the ridge waveguide was formed by partially etching 130 nm Si. Then, separate masks were used to implant boron and phosphorus into the silicon slab regions to form P + + Ohmic contact and N + + Ohmic contact. The implants were activated via an annealing process at 1030 °C for 5 seconds. Finally, the contact vias and the aluminum interconnects was completed.

3. Characterization

The measurement setup, including tunable laser source, polarization and power meter, were used to characterize the optical performances of the carrier-induced silicon Bragg grating filter. The optical measurements were performed after selecting the transverse electric (TE)

#224043 - $15.00 USD Received 29 Sep 2014; revised 24 Oct 2014; accepted 31 Oct 2014; published 21 Nov 2014

polarization. First, a group of cut-back ridge silicon waveguides were evaluated to extract the coupling loss and propagation loss. Compared to other carrier-induced Bragg gratings, the cut-back ridge silicon waveguides didn't have any implantation. It was fabricated with the carrier-induced Bragg gratings on the same wafer. After deducting the coupling loss, the normalized transmission spectra under the forward and reverse biases are shown in Fig. 4(a) and 4(b), respectively. Without any bias applied, there is a reflected wavelength in the transmission spectrum of carrier-induced Bragg grating filter. The reflected central wavelength is 1590.15 nm. According to the Bragg grating equation, the effective refractive index of this carrier-induced Bragg grating of 2.565 is calculated. The excess optical loss resulted from ion implantation in the Bragg grating filter is about 2.0 dB, in consideration of the propagation loss (2.5 dB/cm) of 400nm-wide undoped ridge Si waveguide. So, the optical excess propagation loss caused by ion implantation is about 10 dB/cm. The measured optical 3-dB bandwidth is 0.45 nm. The extinction ratio is ~19 dB.

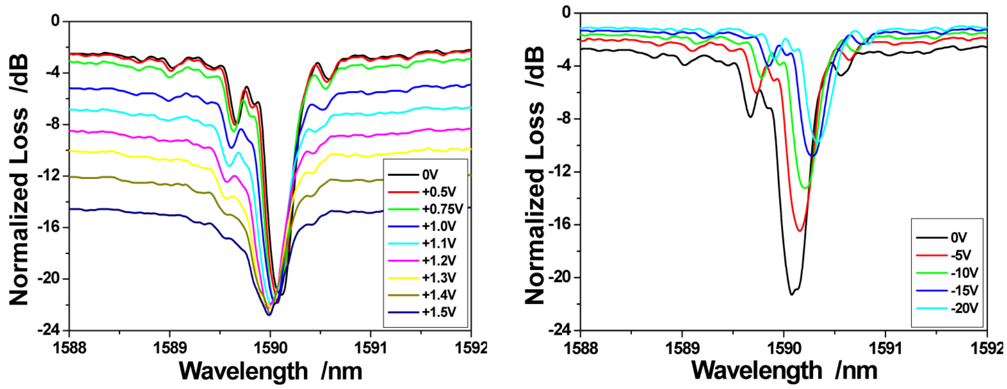

(a) (b)

Fig. 4. Optical transmission spectra of filter. (a) With forward biases. (b) With reverse biases.

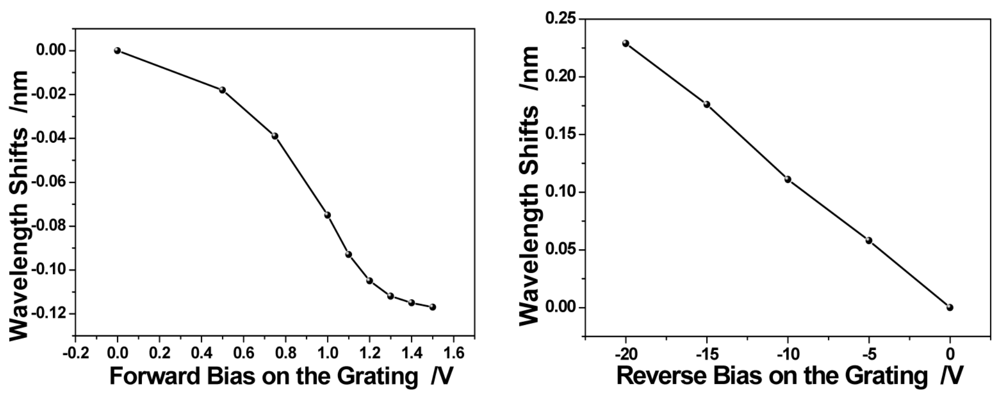

(a) (b)

Fig. 5. Reflected wavelength shifts of filter. (a) With forward biases. (b) With reverse biases.

With increasing the forward bias, the reflected central wavelength is shifted to the short wavelength side. This shift matches the fact that the forward current increases with the applied voltage. According to the carrier plasma dispersion effect, the effective refractive index of the waveguide reduces when the carrier concentration increases. Figure 5(a) shows the central wavelength shift under the different forward biases in details. From 0.5 V to 1.0 V, the plasma dispersion effect dominates the wavelength shift and the central wavelength shifting rates is −1.25 nm/V. When the forward voltage is above 1.1 V, the current is quite

#224043 - $15.00 USD Received 29 Sep 2014; revised 24 Oct 2014; accepted 31 Oct 2014; published 21 Nov 2014

large and the thermo-optic effect also affects the wavelength shift. Thermo-optic effect raises the effective refractive index and the corresponding wavelength moves to the long wavelength side [15]. With the forward current increases, the optical loss increases and the extinction ratio reduces. The increase of the forward current gradually reduces the refractive index difference between the implantation region and the intrinsic region of the carrier-induced Bragg grating. The extinction ratio change of more than 10 dB is realized at the forward voltage of 1.5 V. We reported a PIN-type carrier-induced grating [14]. The depletion width of PIN-type grating under reverse bias is small. The corresponding extinction ratio change is also small. Here, the depletion width of PN-type grating under reverse bias is large and the grating finger can become short under a reverse bias. The length change of grating finger causes the modulation of the extinction ratio of grating. Figure 4(b) shows the spectra of Bragg grating filter under the reverse biases. With increasing the reverse bias, the reflected central wavelength is shifted to the long wavelength side. This is different from the shift direction under the forward bias. Under the reverse bias, the depletion width increases and the carrier concentration decreases near the PN junction. Hence, the effective refractive index of waveguide increases. It causes the reflected wavelength to shift toward the long wavelength side. Moreover, the lower carrier concentration under the reverse bias reduces the optical loss. When the reverse bias is −20 V, the optical loss of this grating reduces to 1.0 dB from 2.5 dB. With increasing of reverse bias, the depletion width at the pn junction increases. Hence, the extinction ratio of grating is modulated. An extinction ratio change of more than 11.5 dB is realized in a bias of −20 V. Figure 5(b) is the corresponding wavelength shift results operated with reverse biases. The wavelength shift rate is ~0.01 nm/V. The modulation frequency of the carrier-induced grating was measured using Agilent N4373C Lightwave Component Analyzer and Agilent B1500A Semiconductor Device Analyzer. The result is shown in Fig. 6(a) when the optical input wavelength of 1590 nm is operated. The 3-dB modulation bandwidth of 5.1 GHz is achieved at the reverse bias of −10 V and the forward RF power of 0 dBm. The IV curve is shown in Fig. 6(b). It shows that the grating is mainly dominated by plasma dispersion effect under the reverse bias because of the small current.

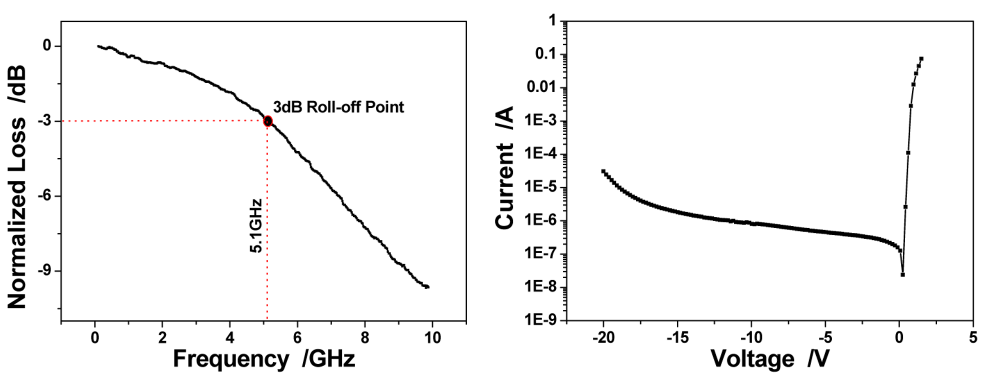

Fig. 6. Electrical performances of grating. (a) 3-dB bandwidth at −10 V. (b) IV curve

4. Conclusion

In conclusion, we demonstrated a PN-type carrier-induced silicon waveguide Bragg formed by ion implantation technology. The bandwidth and the extinction ratio of the grating filter are 0.45 nm and 19 dB, respectively. The extinction ratio modulation is realized under both reverse bias and forward bias. Under the reverse bias, an extinction ratio of more than 11.5 dB is achieved. Under the forward bias, an extinction ratio of more than 10 dB is achieved. The central wavelength shifting rates under forward and reverse biases are −1.25 nm/V and 0.01 nm/V, respectively. The 3-dB modulation bandwidth of this carrier-induced is 5.1 GHz

#224043 - $15.00 USD Received 29 Sep 2014; revised 24 Oct 2014; accepted 31 Oct 2014; published 21 Nov 2014

at a bias of −10 V. With increase the reverse bias, the optical loss reduces. The reduction of optical loss is 1.5 dB under the reverse bias of −20 V. This kind of carrier-induced grating can be used as a special wavelength selective switch. Without any bias, it is used as a normal filter. With a reverse bias, it can guide all waves as a normal waveguide, keeping a low optical loss.

Acknowledgments

The author would like to thank National Natural Science Foundation of China (Grant No. 61177064) and Singapore A*STAR SERC Grant No.1122804038 for support.